J Mater Sci: Mater Med (2015) 26:188
DOI 10.1007/s10856-015-5513-4

Original Research

Akermanite scaffolds reinforced with boron nitride nanosheets in bone tissue engineering

Cijun Shuai[2,3] · Zikai Han[2] · Pei Feng[2] · Chengde Gao[2] · Tao Xiao[3,4] · Shuping Peng[1,5]

Received: 11 December 2014 / Accepted: 16 March 2015 / Published online: 28 April 2015

Abstract Akermanite (AKM) is considered to be a promising bioactive material for bone tissue engineering due to the moderate biodegradability and excellent biocompatibility. However, the major disadvantage of AKM is the relatively inadequate fracture toughness, which hinders the further applications. In the study, boron nitride nanosheets (BNNSs) reinforced AKM scaffolds are fabricated by selective laser sintering. The effects of BNNSs on the mechanical properties and microstructure are investigated. The results show that the compressive strength and fracture toughness increase significantly with BNNSs increasing from 0.5 to 1.0 wt%. The remarkable improvement is ascribed to pull out and grain wrapping of BNNSs with AKM matrix. While, overlapping sheets is observed when more BNNSs are added, which results in the decline of mechanical properties. In addition, it is found that the composite scaffolds possess good apatite-formation ability when soaking in simulated body fluids, which have been confirmed by energy dispersed spectroscopy and flourier transform infrared spectroscopy. Moreover, MG63 osteoblast-like cells and human bone marrow stromal cells are seeded on the scaffolds. Scanning electron microscopy analysis confirms that both cells adhere and proliferate well, indicating favorable cytocompatibility. All the facts demonstrate the AKM scaffolds reinforced by BNNSs have potential applications for tissue engineering.

✉ Shuping Peng
shuping@csu.edu.cn

1 Hunan Provincial Tumor Hospital and The Affiliated Tumor Hospital of Xiangya School of Medicine, Central South University, Changsha 410013, China

2 State Key Laboratory of High Performance Complex Manufacturing, Central South University, Changsha 410083, China

3 Orthopedic Biomedical Materials Institute, Central South University, Changsha 410083, China

4 Department of Orthopedics, The Second Xiangya Hospital, Central South University, Changsha 410011, China

5 School of Basic Medical Science, Central South University, Changsha 410078, China

1 Introduction

As one of the most promising biomaterials, akermanite (AKM) possesses excellent apatite mineralization and osteostimulation ability [1, 2]. To be specific, AKM can stimulate the proliferation and differentiation of various kinds of stem cells such as adipose derived stem cells and human aortic endothelial cells [3, 4]. In addition, AKM exhibits unique properties such as accelerating effect of angiogenesis, which contributes to the enhancement of osteogenesis [5]. However, the application of AKM is significantly hindered by its intrinsic low fracture toughness. Actually, the fracture toughness of AKM was only 1.83 MPa $m^{1/2}$, which failed to reach the demanding range of cortical bone [6]. In order to deal with this problem, one feasible method is to incorporate second phase as reinforcement into the matrix.

Boron nitride nanosheets (BNNSs) are one of the most typical two-dimensional nanomaterials with high elastic modulus (~850 GPa), large specific surface area and superb thermal stability [7–9]. The structural, physical and chemical properties make BNNSs suitable candidates for the improvement of mechanical properties. Generally, load transfer and energy dissipation at sheet-matrix interfaces play a vital role in strengthening and toughening the composite, respectively [10, 11]. Besides, boron nitride has

been reported to be biocompatible. Specifically, boron nitride is non-cytotoxic to osteoblasts, macrophages and human embryonic kidney cells (HEK-293) [12–14].

Many research have been carried out on the reinforcing effects and bioactivity of BNNSs. U. Khan added 0.12 vol% BNNSs into a polyvinyl alcohol matrix to prepare the composite and found remarkable improvement in Young's modulus and tensile strength of 40 % compared with the pure polymer [15]. Y. Wang investigated the difference between hexagonal boron nitride and BNNSs based on their effect on mechanical properties when incorporated into polybenzimidazole. The results showed that the modulus increased from 3.3 to 4.2 GPa when 4 wt% BNNSs were incorporated, while the composite added with hexagonal boron nitride remained almost the same [16]. F. Lu demonstrated in vitro application of BNNSs in tissue engineering, biosensor and biosubstance delivery [17]. In addition, D Lahiri found that the apatite formation requires only ~4.6 days of incubation period, indicating good bioactivity of boron nitride [18].

In this study, BNNSs were added into AKM matrix to improve the compressive strength and fracture toughness. BNNSs reinforced AKM scaffolds were fabricated by selective laser sintering. The microstructure and chemical composition were tested by scanning electron microscope (SEM), energy dispersive spectroscopy (EDS) and flourier transform infrared spectroscopy (FTIR). The mechanical properties were investigated and the reinforcing mechanisms were also analyzed. Besides, the apatite formation ability of the scaffolds was confirmed by soaking in simulated body fluids (SBF). Both MG63 cells and human bone marrow stromal cells (BMSCs) was used to study the cytocompatibility of the scaffolds.

2 Materials and methods

2.1 Materials

The AKM powder (size: 5–40 μm, purity: >98 %) was purchased from Kun Shan Chinese Technology New Materials Co. Ltd. In general, the powder was synthesized by sol–gel method and the detailed synthesis process was described as followed [19]. First, the tetraethyl orthosilicate ($(C_2H_5O)_4Si$, TEOS), deionized water and 2 $N{\cdot}HNO_3$ were blended in a mol ratio of 1:8:0.16 ($TEOS:H_2O:HNO_3$) followed by stirring for 30 min at room temperature. Afterwards, $Mg(NO_3)_2{\cdot}6H_2O$ and $Ca(NO_3)_2{\cdot}4H_2O$ were incorporated in the solution in a mol ratio of 1:0.5:1 (TEOS: $Mg(NO_3)_2{\cdot}6H_2O$: $Ca(NO_3)_2{\cdot}4H_2O$) and then stirred for 5 h. Subsequently, the solution was kept in a drying oven at 120 °C for 2 days to obtain the xerogel. The xerogel was sieved to 250-mesh, moved into an alumina crucible and calcined at 1300 °C for 3 h to get the AKM powder. BNNSs (diameter: 0.5–5 μm, thickness: <50 nm, purity: >99.5 %) synthesized by chemical vapor deposition were supplied by Nanjing XF NANO Materials Tech Co., Ltd. The AKM and BNNSs powders were dispersed in alcohol and subjected to sonication for 30 min with a sonicator, followed by ball milling for 8 h. Specifically, various content of BNNSs (0, 0.5, 1.0 and 1.5 wt%) were added into the AKM matrix.

The composite scaffolds were fabricated by a home-made selective laser sintering system [20, 21]. In the study, the parameters were kept as followed: laser power (8 W), scanning speed (150 mm/min), spot diameter (1 mm) and layer thickness (0.15 mm).

2.2 Characterization

The compressive tests were conducted by a universal mechanical tester (Shanghai Zhuoji Instruments Co., Ltd, China) with a 30 N maximum load at a crosshead speed of 0.5 mm/min. The load was applied perpendicular to each scaffold. Five samples per group were tested, and the means and standard deviations were calculated. Besides, the fracture toughness and hardness of the scaffolds were tested by the Vickers microindenter (HXD-1000TM/LCD, Digital Micro Hardness Tester, Shanghai Taiming Optical Instrument Co., Ltd, China). For the test, experimental specimens of the composite scaffolds in the shape of rectangular bars with dimensions of 5 mm thickness, 8 mm height and 20 mm length were made. The fracture toughness Kic was calculated by the equation which was proposed by Evans as followed [22]:

$$\mathrm{Kic} = 0.0824\mathrm{Pc}^{-3/2}$$

where P is the indentation load and c is the length of the induced crack. Similarly, five specimens per group were tested.

The microstructure was investigated by SEM (JEOL, JSM-6490LA, Japan) at an accelerating voltage of 20.0 kV. Before observation, the samples were sputter-coated with gold for 120 s under vacuum. Besides, the element analysis was performed by SEM equipped with an EDS detector. Chemical structure was investigated using a Fourier transform infrared spectrometer (FTIR) (NicoletteTM 6700, Thermo Electron Corp., USA) at a wavenumber range of 400–4000 cm^{-1} and with a resolution of 2 cm^{-1}.

2.3 SBF

The apatite nucleation on the scaffolds was examined under static mineralisation conditions according to Kokubo's protocol [23]. The scaffolds were immersed in polyethylene bottle containing 50 mL of SBF solution at 37 °C. The SBF

contained (in mM) Na^+(142), K^+(5.0), Mg^{2+}(1.5), Ca^{2+}(2.5), Cl^-(147.8), HCO^{3-}(4.2), $SO_4{}^{2-}$(0.5) and $HPO_4{}^{2+}$(1.0) and had a pH of 7.4 which was adjusted by Tris(hydroxymethyl)aminomethane and HCl. The culture time was determined to 14 and 28 days. After specified time, the scaffolds were collected from SBF medium, rinsed with distilled water and dried in air at room temperature. The surface and cross-section was visualized by SEM. The formation of apatite layer was confirmed by EDS and FTIR.

2.4 Cell culture

Human osteosarcoma cell line MG63, which was obtained from ATCC no. CRL-1427, Rockville, MD, USA, and BMSCs, which were isolated from the adult human bone marrow aspirates of ribs of patients undergoing thoracic surgery, were used to investigate cytocompatibility of the scaffolds. MG63 cells are derived from human osteosarcoma tissue and exhibited lots of characteristic features of osteoblasts. The sample collection of BMSCs was approved by the patients with signed informed consent forms and the ethical review committees of Second Xiangya Hospital. BMSCs are one of the most typical stem cell to due to the good capability of differentiation into various cell lineages, especially osteogenic cell. Both cells were cultured in 75 cm^2 flask at 37 °C in a humidified incubator with 5 % CO_2. The culture medium was Dulbecco's Modified Eagle's Medium (DMEM, Invitrogen Life Technologies, Karlsruhe, Germany) supplemented with 10 % fetal bovine serum (FBS) and antibiotics (100 U/ml penicillin and 100 mg/ml streptomycin). When reaching 80–90 % confluence, the cells were trypsinized and counted using a hemacytometer. Meanwhile, the scaffolds were sterilized under UV radiation for 2 h, rinsed three times with PBS and soaked in MEM for 24 h before cell seeding. Subsequently, 50 µl suspension containing 1×10^5 cells were seeded on the scaffolds, followed by incubation for 2 h in 24-well culture plates to allow for cell adhesion. After 1, 3, 5 and 7 days of incubation, the scaffolds seeded with cells were collected from the medium, washed with PBS and fixed with 4 % glutaraldehyde for 4 h. Then, the scaffolds were dehydrated through a series of graded ethanol (30, 50, 70, 90, 100 %), reeze-dried overnight and analyzed by SEM.

2.5 Statistical analysis

All quantitative data for compressive strength and fracture toughness were obtained from samples in quintuplicate and expressed as ± standard deviation (SD). Statistical analysis was performed using SPSS (Statistical Package for the Social Sciences) software (SPSS Statistics version 19, IBM, Armonk, NY, USA). A value of $P < 0.05$ was considered to be statistically significant and $P < 0.01$ remarkably significant.

3 Results and discussions

3.1 Microstructure

The fracture surfaces of the scaffolds with different content of BNNSs are shown in Fig. 1. When 0.5 wt% BNNSs were incorporated, it was clear that BNNSs wrapped along the grain and embedded firmly in the AKM matrix (Fig. 1a). With the BNNSs increasing to 1.0 wt%, the number of BNNSs increased and distributed homogeneously on the fracture surface (Fig. 1b). For the scaffolds with 1.5 wt%, BNNSs aggregated and overlapped, leading to some flaws such as pores and cracks (Fig. 1c). High-magnification image in Fig. 1d showed that BNNSs pulled out in the fracture zone with the plane of the sheets perpendicular to that of the fracture surface.

3.2 Mechanical properties

The compressive strength and fracture toughness of the scaffolds with various contents of BNNSs are shown in Fig. 2. The compressive strength increased with BNNSs increasing to 1.0 wt%, thereafter decrease with further increasing of BNNSs content. The optimum compressive reached 12.13 ± 0.67 MPa, which had an increase of 105 % than that of pure AKM ceramics. When more BNNSs were incorporated, the compressive decreased to 10.33 ± 0.49 MPa. On the other hand, the fracture toughness exhibited similar trend. The initial value was 1.93 ± 0.06 MPa $m^{1/2}$ for the scaffolds with 0.5 wt% BNNSs. Then the fracture toughness reached 2.25 ± 0.08 MPa $m^{1/2}$ and descend to 2.08 ± 0.04 MPa $m^{1/2}$, respectively. Due to the favorable mechanical properties of the scaffolds with 1.0 wt% BNNSs, the scaffolds was used to investigate the following in vitro bioactivity test and cell culture.

The improvement of mechanical properties of the AKM-BNNSs composite scaffold was ascribed to the BNNSs' large specific surface area, high aspect ratio, excellent mechanical properties and their capacity to protrude from the surface in a more effective way than 0-dimensional and 1-dimensional additives. Specifically, when crack propagated, it needed to overcome resistance to run through grain boundaries in AKM matrix. Then, crack spread along sheet/matrix interface and overcomes the shear resistance to make BNNSs debond and pull out. It should be noted that the shear strength increased with the crack opening displacement increasing before pulling-out. The toughening mechanism consumed a large amount of

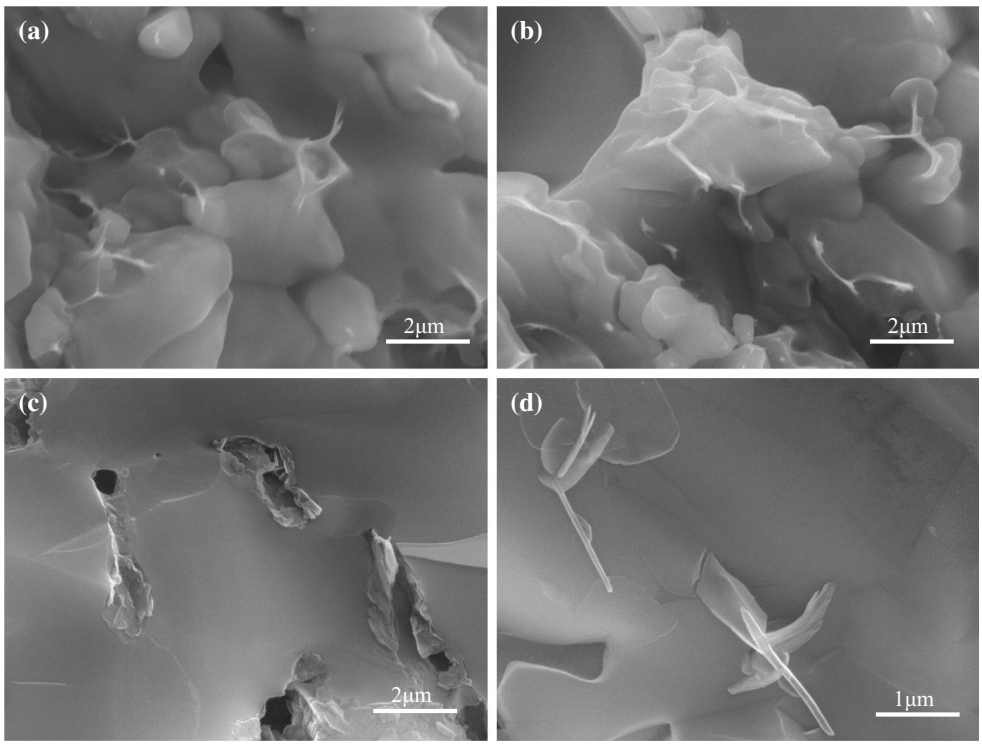

Fig. 1 SEM micrographs of fracture surfaces of BNNSs reinforced AKM scaffolds. **a** 0.5 wt% BNNSs **b** 1.0 wt% BNNSs **c** 1.5 wt% BNNSs and **d** high magnification micrographs of fracture surfaces of AKM-1.0BNNSs scaffold revealing protruding out of BNNSs with AKM matrix

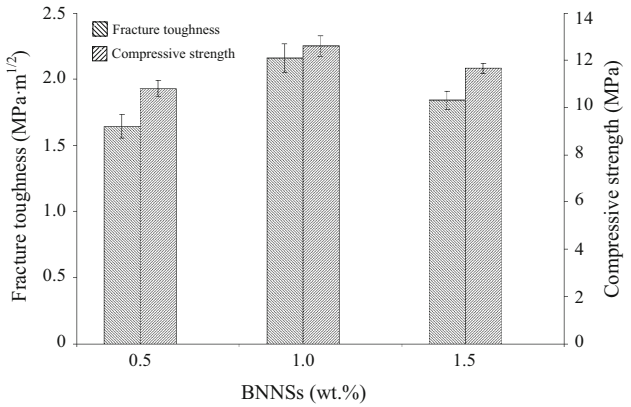

Fig. 2 Effects of BNNSs on compressive strength and fracture toughness of the composite scaffolds. (n = 5, $P < 0.05$)

energy and improved the fracture toughness of the scaffolds. In general, the energy needed to pull out sheets in greater than that of particles and whiskers because of sheet wrapping around the grain boundary and the resulting larger contact area with the matrix. Moreover, grain wrapping prevented crystal grain growth and facilitated more effective sintering due to high thermal and electrical conductivity of BNNSs. The organized BNNSs networks promoted energy dissipation and further toughened the composites. In addition, the mismatch of thermal expansion coefficient between AKM ($\sim 5.6 \times 10^{-6}\ K^{-1}$) and BNNSs ($2.0 \times 10^{-6}\ K^{-1}$) resulted in abundant residual stress at the interface when the composites were cooled to room temperature after sintering. An isostatic tensile stress to the AKM grains was then produced, which would delay the crack of the matrix. However, sheet overlapping and the resulting flaws such as pores and cracks weakened the mechanical properties of the scaffolds.

3.3 SBF

The scaffolds after soaking in SBF for 14 and 28 days are shown in Fig. 3a, b. After 14 days of immersion, a large amount of crystalline deposition was homogenously distributed on the surface. High-magnification image showed that the newly formed layer was composed of nanocrystals with flake-like structure (Fig. 3a). After 28 days, the cohesive depositions exhibited characteristic cauliflower-like morphology, which was derived from the agglomeration of crystals. The diameter of apatite-like clusters was up to 2 μm in the high-magnification image (Fig. 3b). Besides, the cross-section images of the scaffolds after various days of culture are shown in Fig. 3c, d. It should be noted that the thickness of the formed layer was relatively small after 14 days, while the thickness increased and reached about 13 μm after 28 days. The EDS spectra of the scaffolds after immersing in SBF are shown in Fig. 3e, f. It could be analyzed that with the soaking time increasing, the Si and Mg intensity decreased, while the P intensity increased continuously. The fact resulted in the decrease of Ca/P

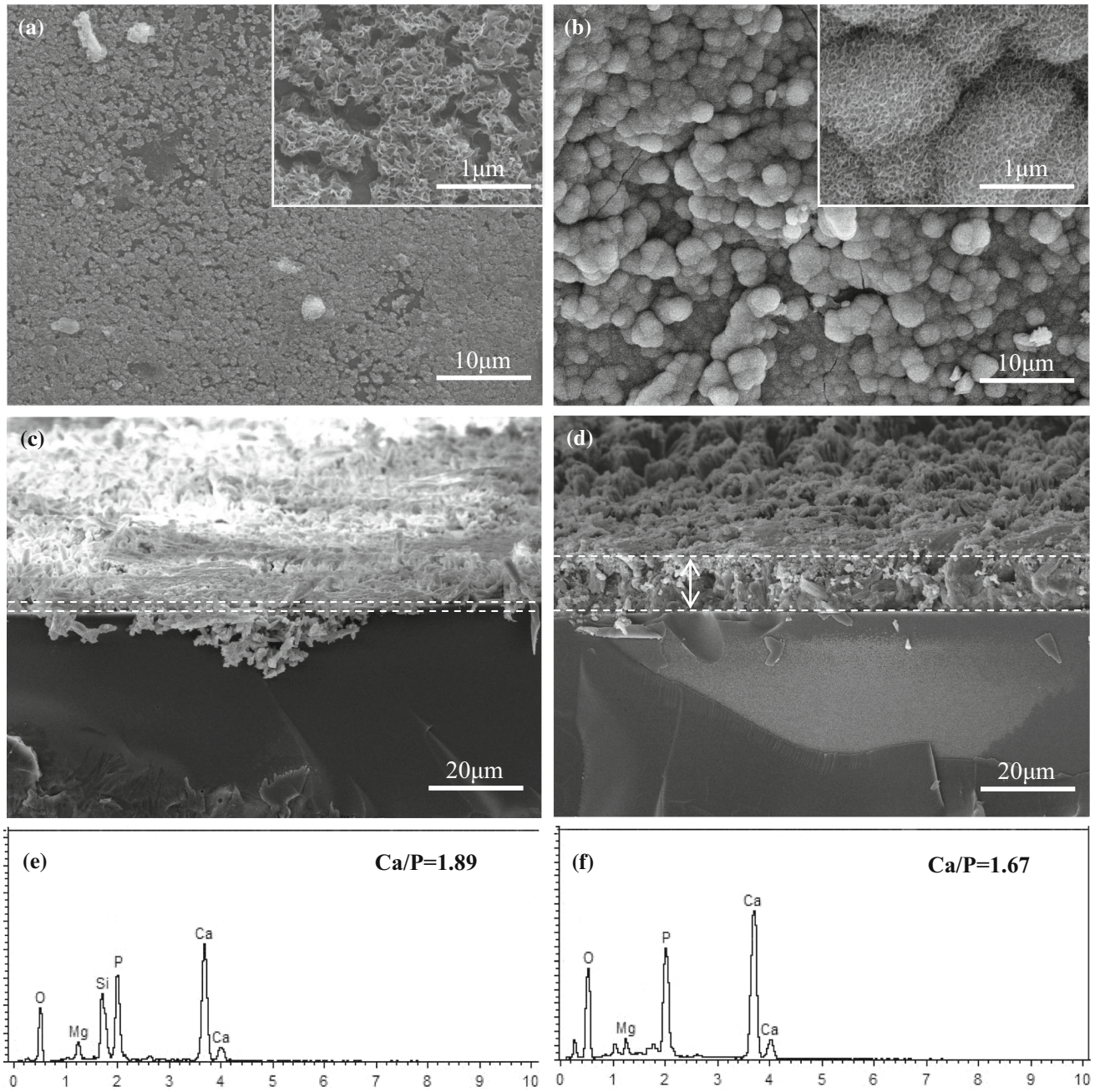

Fig. 3 SEM microphotographs of the scaffolds after soaking in SBF for **a** 14 and **b** 28 days. Cross-section images after **c** 14 and **d** 28 days of culture. EDS spectra of the scaffolds after **e** 14 and **f** 28 days of immersion

ratio. The value reached 1.67 after 28 days, which was close to the stoichiometric ratio of hydroxyapatite (1.63).

The ions exchange and apatite formation process could be interpreted as followed. When the scaffolds was immersed in the SBF, Ca^{2+} dissolved from AKM exchanged with H^+ in the solution, leading to a pH increase of SBF solution, which further led to the formation of a hydrated silica gel layer on the surface of the scaffolds: Si–O-Ca-O-Si + $2H^+ = 2$ Si–OH + Ca^{2+}. The silica gel layer composed of abundant functional silanol (Si–OH) groups offered favorable sites for calcium phosphate nucleation [24]. Moreover, final production of a negatively charged surface with the functional group (Si–O^-) formed: Si–OH + OH^-= Si–O^- + H2O. It had been reported that the electrostatic interaction is an important factor in inducing Ca–P nucleation, and this type of nucleation could mainly formed on a negatively charged interface [25]. In detail, the formed Si–O^- could interact with positively charged Ca^{2+}

ions to form a Ca-rich positive thin layer, and finally combine with negatively charged PO_4^{3-} ions to form amorphous calcium phosphate, which transforms into apatite in SBF: $10Ca^{2+} + 6PO_4^{3-} + 2OH^- = Ca_{10}(PO_4)_6(OH)_2$ [26].

The FTIR spectra of the scaffolds before and after immersion in SBF for 14 and 28 days are presented in Fig. 4. Before soaking in SBF, silicate absorption bands were observed at the wavenumber of 1010, 972, 930, 850, 639, 586 and 474 cm^{-1} in the spectra (Fig. 4c) [27]. After soaking in SBF, the peak at 1600 cm^{-1} was attributed to the O–H bond of the hydroxyl groups [28]. Besides, the gradual formation of phosphate absorption bands at 1100, 601 and 563 cm^{-1} appeared [29]. With the immersion time increasing, the peaks at 3600 and 1600 cm^{-1} increase in intensity, indicating the formation of hydroxyapatite on the scaffolds [30]. In addition, the peaks located at 1400 cm^{-1} was assigned to vibration of the C–O bond on the carbonate groups, which confirmed the existence of carbonated hydroxyapatite [31]. In general, the apatite mineralization ability has a direct correlation with the dissolution of the materials [32]. When the scaffolds soaked in simulated body fluid (SBF), there exists the release of ions and ionic products, such as Ca^{2+}, Mg^{2+}, Si^{2+} and Si–OH, which provide the nucleation sites for apatite mineralization [33]. Besides, AKM possesses a moderate degradation rate, which helps to create favorable biological conditions, including proper ionic concentrations and pH value [34]. All the facts demonstrated that the scaffolds possessed favorable apatite formation ability.

3.4 Cell culture

The images of MG63 cells are observed by SEM after 1, 3, 5 and 7 days of incubation on the scaffolds. As seen in Fig. 5a, cells showed an elongated shape and adhered to the substrates after 1 day of cultivation. Besides, long filopodia and broad lamellipodia protrude from the cell body, indicating intimate attachment with the scaffolds. After 3 days, the majority of the cell gathered together and the others scattered randomly on the surface (Fig. 5b). After 5 days, the number and size of the cells increased dramatically (Fig. 5c). After 7 days, the cell layer became increasingly confluent and nearly covered the entire surface of the scaffolds (Fig. 5d).

The images of the scaffolds seeded with BMSCs for 1, 3, 5 and 7 days are depicted in Fig. 6. After 1 day of incubation, BMSCs began to adhere and spread with a flattened morphology (Fig. 6a). After 3 days, BMSCs exhibited a spindle-like appearance with cellular processes (lamellipodia and filopodia) attached to the underlying matrix. Besides, abundant extracellular matrix (ECM) is secreted by BMSCs and overlapped the surface of scaffolds. It should be highlighted that ECM was not merely conducive to the foundation for tissue growth, but also a dynamic participant in cellular crosstalk (Fig. 6b). As the culture time increased to 5 days, both number and size of BMSCs increased (Fig. 6c). By day 7, BMSCs aggregated to form cell clusters and covered the entire surface (Fig. 6d). As with the osteostimulation ability of the scaffolds, previous studies demonstrated that Si and Mg containing ions products from AKM also could promote cell

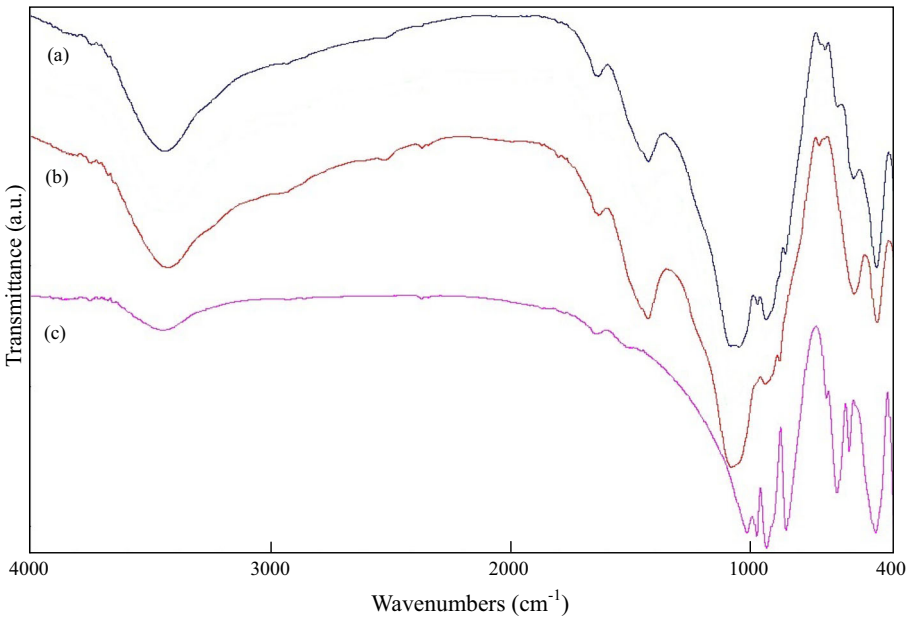

Fig. 4 FTIR spectra of the scaffolds before and after soaking in SBF *a* 14, *b* 28 days, and *c* raw powders

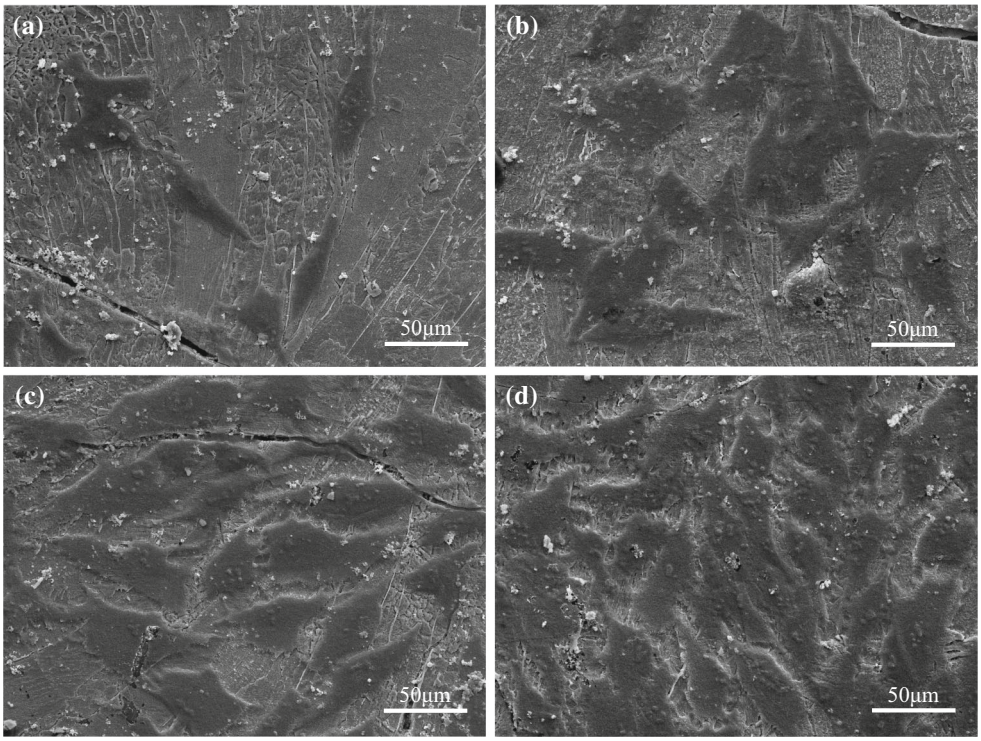

Fig. 5 SEM images of MG63 cells seeded scaffolds for **a** 1, **b** 3, **c** 5 and **d** 7 days

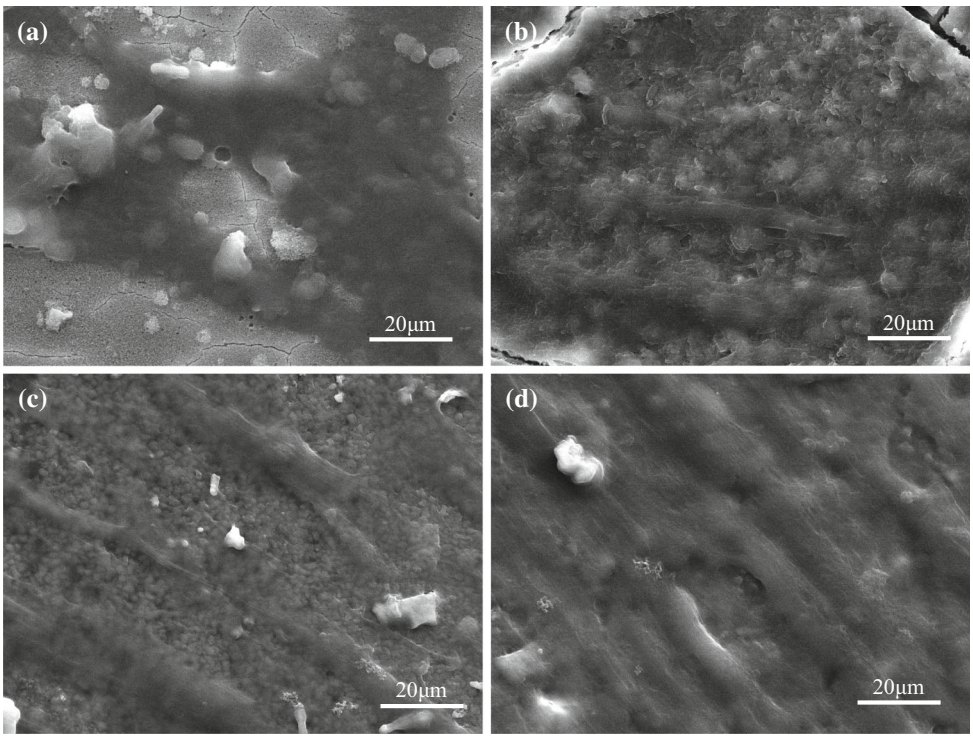

Fig. 6 SEM images of BMSCs seeded scaffolds for **a** 1, **b** 3, **c** 5 and **d** 7 days

attachment and proliferation [35]. Moreover, the apatite mineralization on the surface of the scaffolds plays a vital role in improving osteoblast growth and differentiation [36].

In general, the paper focuses on the mechanical and biological properties of the AKM scaffolds reinforced with BNNSs. Actually, the dynamic mechanical properties are also important. These properties indicated the mechanical

stability of the scaffolds in vitro and in vivo. Besides, we should find ways to improve the dispersing performance of BNNSs in ceramic matrix, which will further increase the mechanical properties. Introducing one-dimensioned nano materials to the AKM-BNNSs system may be a feasible method to realize this.

4 Conclusions

In the research, AKM scaffolds reinforced with BNNSs were fabricated by selective laser sintering. The influence of BNNSs on microstructure and mechanical properties were evaluated. The results showed that both compressive strength and fracture toughness increased and then descend when BNNSs were incorporated. The improvement of mechanical properties were ascribe to sheet pull-out, grain wrapping and mismatch of thermal expansion coefficient. While, when more BNNSs were added, sheet overlapping and the resulting flaws appeared. Moreover, apatite was formed on the scaffolds and increased with the culture time increasing in SBF medium. Furthermore, both MG63 cells and BMSCs adhere and spread well on the scaffolds, indicating excellent biocompatibility of the scaffolds.

Acknowledgments This work was supported by the following funds: (1) The Natural Science Foundation of China (51222506, 81372366, 81472058); (2) Overseas, Hong Kong & Macao Scholars Collaborated Researching Fund of National Natural Science Foundation of China (81428018); (3) Hunan Provincial Natural Science Foundation of China (14JJ1006); (4) Project supported by the Fok Ying-Tong Education Foundation, China (131050); (5) Shenzhen Strategic Emerging Industrial Development Funds (JCYJ20130401160614372); (6) The Open-End Fund for the Valuable and Precision Instruments of Central South University; (7) The faculty research grant of Central South University (2013JSJJ011, 2013JSJJ046); (8) State Key Laboratory of New Ceramic and Fine Processing Tsinghua University (KF201413).

References

1. Ni S, Chang J, Chou L. In vitro studies of novel $CaO–SiO_2–MgO$ system composite bioceramics. J Mater Sci Mater Med. 2008;19:359–67.
2. Ventura JMG, Tulyaganov DU, Agathopoulos S, Ferreira JMF. Sintering and crystallization of akermanite-based glass–ceramics. Mater Lett. 2006;60:1488–91.
3. Liu Q, Cen L, Yin S, Chen L, Liu G, Chang J, Cui L. A comparative study of proliferation and osteogenic differentiation of adipose-derived stem cells on akermanite and β-TCP ceramics. Biomaterials. 2008;29:4792–9.
4. Zhai W, Lu H, Wu C, Chen L, Lin X, Naoki K, Chen G, Chang J. Stimulatory effects of the ionic products from Ca–Mg–Si bioceramics on both osteogenesis and angiogenesis in vitro. Acta Biomater. 2013;9:8004–14.
5. Huang Y, Jin X, Zhang X, Sun H, Tu J, Tang T, Chang J, Dai K. In vitro and in vivo evaluation of akermanite bioceramics for bone regeneration. Biomaterials. 2009;30:5041–8.
6. Wu C, Chang J. A novel akermanite bioceramic: preparation and characteristics. J Biomater Appl. 2006;21:119–29.
7. Yurdakul H, Göncü Y, Durukan O, Akay A, Seyhan AT, Ay N, Turan S. Nanoscopic characterization of two-dimensional (2D) boron nitride nanosheets (BNNSs) produced by microfluidization. Ceram Int. 2012;38:2187–93.
8. Fang X, Fan L, Ding Q, Yao X, Wu Y, Hou J, Wang X, Yu Z, Cheng G, Hu Y. Thermal energy storage performance of paraffin-based composite phase change materials filled with hexagonal boron nitride nanosheets. Energy Convers Manag. 2014;80:103–9.
9. Lei W, Zhang H, Wu Y, Zhang B, Liu D, Qin S, Liu Z, Liu L, Ma Y, Chen Y. Oxygen-doped boron nitride nanosheets with excellent performance in hydrogen storage. Nano Energy. 2014;6:219–24.
10. Li D, Wang X, Liu W, Wu K, Shi H, Ding C, Hu X, Zheng M. Microstructure and strengthening mechanism of carbon nanotubes reinforced magnesium matrix composite. Mater Sci Eng A. 2014;597:264–9.
11. Zhang X, Alloul O, He Q, Zhu J, Verde MJ, Li Y, Wei S, Guo Z. Strengthened magnetic epoxy nanocomposites with protruding nanoparticles on the graphene nanosheets. Polymer. 2013;54:3594–604.
12. Lahiri D, Singh V, Benaduce AP, Seal S, Kos L, Agarwal A. Boron nitride nanotube reinforced hydroxyapatite composite: mechanical and tribological performance and in vitro biocompatibility to osteoblasts. J Mech Behav Biomed. 2011;4:44–56.
13. Lahiri D, Rouzaud F, Richard T, Keshri AK, Bakshi SR, Kos L, Agarwal A. Boron nitride nanotube reinforced polylactide–polycaprolactone copolymer composite: mechanical properties and cytocompatibility with osteoblasts and macrophages in vitro. Acta Biomater. 2010;6:3524–33.
14. Turco SD, Ciofani G, Cappello V, Gemmi M, Cervelli T, Saponaro C, Nitti S, Mazzolai B, Basta G, Mattoli V. Cytocompatibility evaluation of glycol-chitosan coated boron nitride nanotubes in human endothelial cells. Colloids Surf B. 2013;111:142–9.
15. Khan U, May P, Neil AO, Bell AP, Boussac E, Martin A, Semple J, Coleman JN. Polymer reinforcement using liquid-exfoliated boron nitride nanosheets. Nanoscale. 2013;5:581–7.
16. Wang Y, Shi Z, Yin J. Boron nitride nanosheets: large-scale exfoliation in methanesulfonic acid and their composites with polybenzimidazole. J Mater Chem. 2011;21:11371–7.
17. Lu F, Wang F, Cao L, Kong C, Huang X. Hexagonal boron nitride nanomaterials: advances towards bioapplications. Nanosci Nanotechnol Lett. 2012;4:949–61.
18. Lahiri D, Singh V, Keshri AK, Seal S, Agarwal A. Apatite formability of boron nitride nanotubes. Nanotechnology. 2011;22:205601.
19. Razavi M, Fathi M, Savabi O, Razavi SM, Beni BH, Vashaee D, Tayebi L. Controlling the degradation rate of bioactive magnesium implants by electrophoretic deposition of akermanite coating. Ceram Int. 2014;40:3865–72.
20. Gao C, Liu T, Shuai C, Peng S. Enhancement mechanisms of graphene in nano-58S bioactive glass scaffold: mechanical and biological performance. Sci Rep. 2014;4:4712.
21. Feng P, Niu M, Gao C, Peng S, Shuai C. A novel two-step sintering for nano-hydroxyapatite scaffolds for bone tissue engineering. Sci Rep. 2014;4:5599.
22. Ercenk E, Sen U, Yilmaz S. The effect of bond coat composition on oxidation behavior of basalt base glass and glass–ceramics. Surf Coat Technol. 2013;232:703–9.
23. Torres FG, Nazhat SN, Fadzullah SM, Maquet V, Boccaccini AR. Mechanical properties and bioactivity of porous PLGA/TiO_2 nanoparticle-filled composites for tissue engineering scaffolds. Compos Sci Technol. 2007;67:1139–47.

24. Yazdimamaghani M, Razavi M, Vashaee D, Pothineni VR, Rajadas J, Tayebi L. Significant degradability enhancement in multilayer coating of polycaprolactone-bioactive glass/gelatin-bioactive glass on magnesium scaffold for tissue engineering applications. Appl Surf Sci. 2015;. doi:10.1016/j.apsusc.2015.02.120.
25. Park H, Choi B, Nguyen J, Fan J, Shafi S, Klokkevold P, Lee M. Anionic carbohydrate-containing chitosan scaffolds for bone regeneration. Carbohydr Polym. 2013;97:587–96.
26. Wu Z, Tang T, Guo H, Tang S, Niu Y, Zhang J, Zhang W, Ma R, Su J, Liu C, Wei J. In vitro degradability, bioactivity and cell responses to mesoporous magnesium silicate for the induction of bone regeneration. Colloids Surf B. 2014;120:38–46.
27. Chen L, Zhai D, Wu C, Chang J. Poly(d, l-lactic)-reinforced akermanite bioceramic scaffolds: preparation and characterization. Ceram Int. 2014;40:12765–75.
28. Blber MV, Stumm W. An in situ ATR-FTIR study: the surface coordination of salicylic acid on aluminum and iron (III) oxides. Environ Sci Technol. 1994;28:763–8.
29. Yi D, Wu C, Ma X, Heng J, Zheng X, Chang J. Preparation and in vitro evaluation of plasma-sprayed bioactive akermanite coatings. Biomed Mater. 2012;7:5004.
30. Antonakos A, Liarokapis E, Leventouri T. Micro-Raman and FTIR studies of synthetic and natural apatites. Biomaterials. 2007;28:3043–54.
31. Slosarczyk A, Paszkiewicz Z, Paluszkiewicz C. FTIR and XRD evaluation of carbonated hydroxyapatite powders synthesized by wet methods. J Mol Struct. 2005;744:657–61.
32. Wu C, Chang J. Degradation, bioactivity, and cytocompatibility of diopside, akermanite, and bredigite ceramics. J Biomed Mater Res Appl Biomater. 2007;83:153–60.
33. Gu H, Guo F, Zhou X, Gong L, Zhang Y, Zhai W, Chen L, Cen L, Yin S, Chang J, Cui L. The stimulation of osteogenic differentiation of human adipose-derived stem cells by ionic products from akermanite dissolution via activation of the ERK pathway. Biomaterials. 2011;32:7023–33.
34. Wu C, Ramaswamy Y, Zreiqat H. Porous diopside ($CaMgSi_2O_6$) scaffold: a promising bioactive material for bone tissue engineering. Acta Biomater. 2010;6:2237–45.
35. Sun H, Wu C, Dai K, Chang J, Tang T. Proliferation and osteoblastic differentiation of human bone marrow-derived stromal cells on akermanite-bioactive ceramics. Biomaterials. 2006;27:5651–7.
36. Wu C, Zhai D, Ma H, Li X, Zhang Y, Zhou Y, Luo Y, Wang Y, Xiao Y, Chang J. Stimulation of osteogenic and angiogenic ability of cells on polymers by pulsed laser deposition of uniform akermanite-glass nanolayer. Acta Biomater. 2014;10:3295–306.